XXXth IAU General Assembly, August 2018
Claude Carignan & Danail Obreschkow, ed.
DOI: 10.5281/zenodo.1481554

Baryonic Angular Momentum in Simulated Disks: The CGM

Daniel DeFelippis[1], Shy Genel[2,1], Greg Bryan[1,2]

[1]Department of Astronomy, Columbia University
550 West 120th Street, New York, NY 10027, USA
email: d.defelippis@columbia.edu

[2]Center for Computational Astrophysics, Flatiron Institute
162 Fifth Avenue, New York, NY 10010, USA

Abstract. Physical processes that occur the circumgalactic medium (CGM) are largely responsible for setting the baryonic angular momentum of simulated galaxies. However, the angular momentum of the CGM has yet to be characterized in a large cosmological simulation, which are now capable of reproducing observed angular momentum properties for large populations of galaxies. We present a first step towards understanding the angular momentum properties of the CGM statistically for galaxies in the IllustrisTNG simulation. We focus on Milky Way-mass halos at $z = 0$, but plan to extend this analysis to other masses and redshifts in future work.

Keywords. galaxies: kinematics and dynamics, galaxies: structure, hydrodynamics, methods: numerical

1. Introduction

The stellar specific angular momentum (j_*) and stellar mass (M_*) relation for disk galaxies has been well established since the 1980s observationally (Fall 1983; Fall & Romanowsky 2013), but only relatively recently have simulations been able to reproduce this relation for a large population of galaxies (e.g. Genel et al. 2015; Zavala et al. 2016). Simulations accomplish this with physically motivated feedback models that affect the dynamics of the baryons in many ways, such as by ejecting material in galactic fountains (e.g. Christensen et al. 2016), resulting in a $j_* - M_*$ relationship at $z = 0$ consistent with observations.

DeFelippis et al. (2017) investigated the effect of feedback in shaping the angular momentum of stellar disks in the Illustris simulation by performing a Lagrangian analysis of the $z = 0$ stars in Milky Way-mass galaxies. By tracing the $z = 0$ stars back through time and keeping track of their angular momentum, we found three periods during which feedback operates in different ways. First, feedback lessens angular momentum losses when gas accretes onto the dark matter halo and travels towards the galaxy (compared to a galaxy of the same mass simulated without feedback). Second, feedback causes angular momentum gains via galactic winds by successively ejecting accreted gas from the disk into the CGM. Finally, feedback halts angular momentum losses right before gas forms stars within the disk.

One of our main conclusions was that feedback within the CGM (i.e. during the first two periods defined above) is very important for setting the angular momentum of the enclosed galaxies. There have been many recent efforts to characterize the dynamics of the CGM with both observations (e.g. Turner et al. 2017) and simulations (e.g. Stevens et al. 2017), but no one has yet used a large cosmological simulation to create a comprehensive picture of the angular momentum in the CGM. We are thus motivated to do so using the Illustris and IllustrisTNG simulations.

2. Methods

Illustris (Genel et al. 2014; Vogelsberger et al. 2014a,b) and IllustrisTNG (Marinacci et al. 2018; Naiman et al. 2018; Nelson et al. 2018; Pillepich et al. 2018b; Springel et al. 2018) are large hydrodynamical simulations run in a $\approx(100\ \mathrm{Mpc})^3$ volume using the moving-mesh code AREPO (Springel 2010). In this work, we use the newer IllustrisTNG simulation, which contains models for stellar (Pillepich et al. 2018a) and AGN feedback (Weinberger et al. 2017) which match observational constraints better than the original Illustris feedback prescriptions do (see e.g. Nelson et al. 2018).

We select galaxies from IllustrisTNG in the mass range $10^{11.75} < \mathrm{M_{halo}[M_\odot]} < 10^{12.25}$ at $z = 0$ and calculate j_* of the central galaxies as follows:

$$\mathbf{j}_* = \frac{1}{M_*} \sum_{i=1}^{N} m_{*,i}(\mathbf{r}_{*,i} \times \mathbf{v}_{*,i}) \tag{2.1}$$

where $m_{*,i}$ and M_* are the mass of individual star particles and the total stellar mass respectively, the radius $\mathbf{r}_{*,i}$ is measured from the position of the most bound particle in the galaxy, and the velocity $\mathbf{v}_{*,i}$ is measured in the center of mass frame of the stars. We define a disk galaxy as one that is in the upper quartile of the j_* distribution, as a high value of j_* for a given stellar mass has been shown to be a proxy for morphological disks, both observationally (Fall & Romanowsky 2013) and in simulations (Genel et al. 2015).

For our high-j_* sample, we remove the innermost region of the halo that contains 95% of the stars and dense star-forming gas, and call the remaining gas the CGM. In order to determine the effect of temperature, we divide the CGM into hot and cold phases with a cutoff at half of the virial temperature of the halo ($\sim 10^5$ K for our mass range), and calculate j_{CGM} for those phases in the same reference frame as the calculation of j_*.

3. Results

In this section, we describe properties of our sample of high-j_* galaxies. In Figure 1, we show the position of the high-j_* galaxies' cold and hot CGM on the specific angular momentum-mass ($j - M$) plane. Two key differences are apparent: first, the cold phase typically contains more mass and angular momentum than the hot phase, and second, there is a correlation present in the cold phase that does not appear in the hot phase. From these differences we can deduce properties of the CGM. Cold gas in the CGM is also closer to the galaxy than the hot CGM gas is, which implies that the cold phase must be rotating much more significantly than the hot phase. The correlation present in the cold phase may simply be a consequence of the large extended structures cold gas forms, which both contain a lot of angular momentum and require a lot of mass to sustain themselves.

In Figure 2, we show the magnitudes and directions of the CGM angular momentum vectors with respect to their corresponding stellar angular momentum vectors. Unlike in Figure 1, the two plots are very similar: the alignment angles of the hot and cold phases for this galaxy sample are usually small (median $\approx 20^\circ$) and nearly identical to each other. In other words, despite the difference in rotational velocity magnitudes between the hot and cold gas, they are nevertheless both aligned to the stars in a similar way.

In Figure 3, we try to understand this similarity on a galaxy-by-galaxy basis by comparing the alignments of the hot and cold phases for each galaxy in our high-j_* sample and a corresponding low-j_* sample (the lower quartile of the j_* distribution) from the same halo mass bin. We see that both hot and cold phase alignments with respect to the stars for the low-j_* galaxies are nearly uniformly distributed over all possible angles (me-

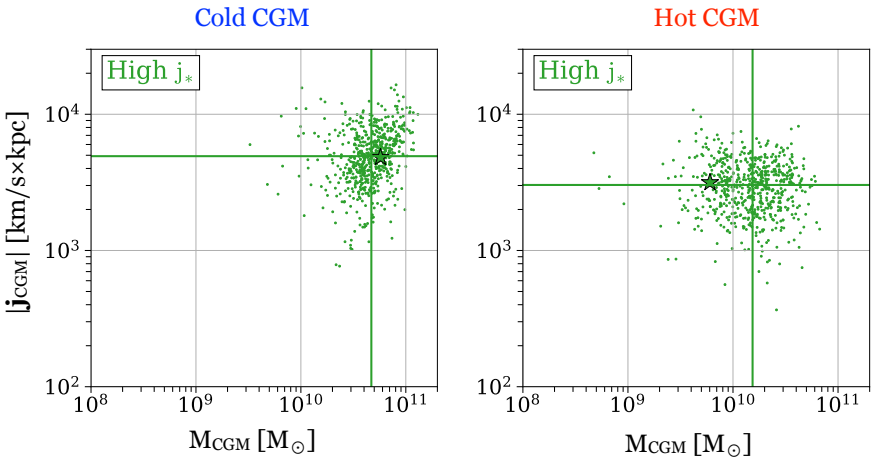

Figure 1. *Left*: Specific angular momentum of the cold phase of the CGM vs. mass of the cold phase. Vertical and horizontal green lines show the medians of the x and y-axis distributions respectively. The outlined star corresponds to a galaxy shown in 3D during the talk summarized by this proceeding, which can be found at http://gam18.icrar.org/talks/. *Right*: Same as left, but for the hot phase of the CGM.

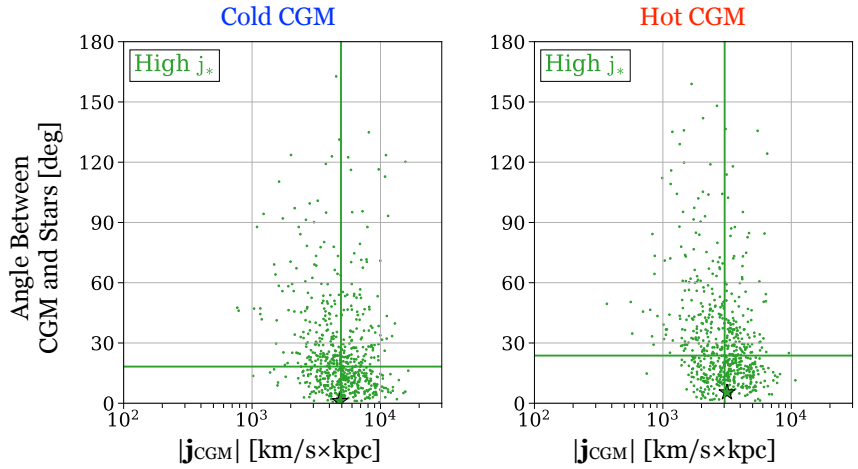

Figure 2. *Left*: Alignment angle of the cold CGM angular momentum vector with respect to the the stellar angular momentum vector vs. magnitude of the cold CGM angular momentum vector. *Right*: Same as left, but for the hot phase of the CGM.

dian $\approx 60°$). These alignment distributions may explain why high-j_* and low-j_* galaxies end up as such: high-j_* galaxies accrete CGM gas that is already mostly aligned to the galaxy, so stars that form out of that gas add to the angular momentum already present, while low-j_* galaxies accrete gas that can be totally misaligned, meaning stars that form may not add to the angular momentum. Additionally, all points are clustered around the 1-1 line (with some scatter), meaning that irrespective of their alignment to the stars, the hot and cold phases of the CGM always coherently rotate with each other.

4. Summary

We selected galaxies from the IllustrisTNG simulation that are in $\sim 10^{12}\mathrm{M}_\odot$ halos at $z = 0$ and examined the angular momentum content of their CGM. We divided the CGM into hot and cold phases to understand what the effect of temperature is. We find

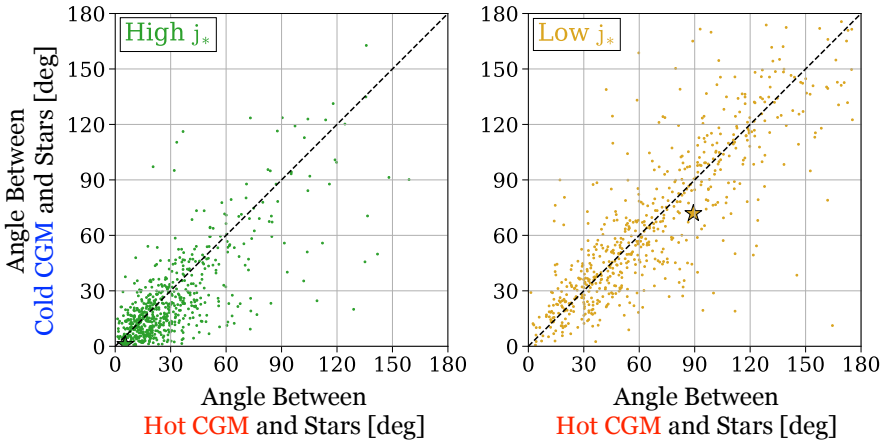

Figure 3. *Left*: Alignment angle between cold gas angular momentum vector and stellar angular momentum vector vs alignment angle between hot gas angular momentum vector and stellar angular momentum vector for high-j_* galaxies. The dotted line is the 1-1 line. *Right*: Same as left but for low-j_* galaxies.

that for galaxies with the highest stellar specific angular momentum, the cold CGM gas contains more mass and more specific angular momentum than the hot CGM gas, but both phases are well aligned to the angular momentum vector of the stars to nearly the same degree. The CGM of low-j_* galaxies is notably not well aligned to the stars, but like the high-j_* galaxies, the hot and cold CGM gas coherently rotate with each other.

All of these $z = 0$ properties suggest particular formation histories, such as hot/cold phase mixing and coherent/non-coherent accretion that may help explain angular momentum growth in the galaxy and the surrounding CGM, which will be investigated as this work continues.

References

Christensen C. R., et al. 2016, *ApJ*, 824, 57
DeFelippis D., Genel S., Bryan G. L., Fall S. M. 2017, *ApJ*, 841, 16
Fall S. M., Efstathiou G. 1980, *MNRAS*, 193, 189
Fall S. M. 1983, *IAU Symp. 100*, 391
Fall S. M., Romanowsky A. J. 2013, *ApJ*, 769, L26
Genel S., et al. 2014, *MNRAS*, 445, 175
Genel S., et al. 2015, *ApJ*, 804, L40
Marinacci F., et al. 2018, *MNRAS*, 480, 5113
Mo H. J., Mao S., White S. D. M. 1998, *MNRAS*, 295, 319
Naiman J. P., et al. 2018, *MNRAS*, 477, 1206
Nelson D., et al. 2018, *MNRAS*, 475, 624
Pillepich A., et al. 2018, *MNRAS*, 473, 4077
Pillepich A., et al. 2018, *MNRAS*, 475, 648
Springel V. 2010, *MNRAS*, 401, 791
Springel V., et al. 2018, *MNRAS*, 475, 676
Stevens A. R. H., et al. 2017, *MNRAS*, 467, 2066
Turner M. L., et al. 2017, *MNRAS*, 471, 690
Vogelsberger M., et al. 2014, *Natur*, 509, 177
Vogelsberger M., et al. 2014, *MNRAS*, 444, 1518
Weinberger R., et al. 2017, *MNRAS*, 465, 3291
Zavala J., et al. 2016, *MNRAS*, 460, 4466